arXiv:1401.8033v2 [nucl-th] 3 Feb 2014

Predicting magic numbers of nuclei with semi-realistic nucleon-nucleon interactions

H. Nakada*and K. Sugiura
Department of Physics, Graduate School of Science and Technology, Chiba University, Yayoi-cho 1-33, Inage, Chiba 263-8522, Japan

February 4, 2014

Abstract

Magic numbers are predicted in wide range of the nuclear chart by the self-consistent mean-field calculations with the M3Y-P6 and P7 semi-realistic NN interactions. The magic numbers are identified by vanishing pair correlations in the spherical Hartree-Fock-Bogolyubov regime. We also identify submagic numbers when energy gain due to the pairing is sufficiently small. It is found that the results with M3Y-P6 well correspond to the known data, apart from a few exceptions. For some of the magic or submagic numbers the prediction differs from that with the Gogny-D1S or D1M interaction. Roles of the tensor force and the spin-isospin channel originating from the one-pion exchange potential are investigated in the Z- or N-dependence of the shell gap.

1 Introduction

The shell structure is one of the fundamental concepts in nuclear physics, which is well described as if the constituent nucleons moved inside the nuclear mean field (MF) almost independently. A large energy gap between the single-particle (s.p.) orbits in the spherically symmetric MF produces a magic number, *i.e.* relative stability of nuclei having a specific proton (Z) or neutron number (N), manifesting the shell structure. It has been disclosed by the experiments using the radioactive beams that the shell structure, and therefore the magic numbers, may depend on Z and N [1]. The magic numbers of nuclei are important in understanding the origin of matters, since elements were synthesized via nuclear reactions which should greatly be influenced by stability of relevant nuclei. For instance, several peaks in the abundance of elements correspond to the magic numbers of N. The magic numbers of nuclei could also be responsible for the existence limit of superheavy elements that have not yet been observed.

For the Z- and N-dependence of the shell structure, which is sometimes called *shell evolution* [2], several possible mechanisms have been pointed out. Since the height of the centrifugal barrier depends on the orbital angular momentum ℓ of the s.p. orbits, the s.p. energies of the loosely bound orbits may have significant ℓ-dependence, possibly influencing the shell evolution [3]. However, there has been no clear evidence that the ℓ-dependence of the s.p. energies gives rise to appearance or disappearance of magic numbers. On the other hand, roles of specific channels in the effective nucleonic interaction have been argued. It has been clarified that the tensor channels are important in the shell evolution [4, 5, 6]. The central spin-isospin channel of the nucleon-nucleon (NN) interaction has also been considered [7]. In addition to the NN interaction, roles of the three-nucleon (NNN) interaction have been investigated [8].

While significance of the tensor force in the shell evolution has been clarified qualitatively in Ref. [4], effects of specific channels on magic numbers should be assessed carefully, because in practice magic numbers emerge via interplay of various channels. One of the authors (H.N.) has developed the M3Y-type semi-realistic NN interactions in a series of articles [9, 10, 11, 12]. By applying the numerical

*E-mail: nakada@c.chiba-u.ac.jp

methods of Refs. [13, 14, 15], the self-consistent Hartree-Fock (HF) and Hartree-Fock-Bogolyubov (HFB) calculations have been implemented with the semi-realistic interactions. Since the interactions explicitly include the tensor force with realistic origin and have reasonable nature on the central spin-isospin channel, the MF approaches employing the semi-realistic interactions provide us with a suitable framework for investigating the magic numbers in wide range of the nuclear chart. A good example is the s.p. level inversion observed from ^{40}Ca to ^{48}Ca, which is reproduced remarkably well by the M3Y-type interactions including the realistic tensor force [6]. Note also that the numerical methods of Refs. [13, 14, 15] have ability to handle loosely bound orbitals. The MF calculations with the semi-realistic interactions have been implemented to investigate the shell structure in neutron-rich Ca and Ni nuclei [5]. In this paper we extensively apply the spherical MF approaches with the semi-realistic interactions, particularly the parameter-sets M3Y-P6 and P7 [12], and predict magic numbers in wide range of the nuclear chart, from relatively light to heavy nuclei including nuclei far off the β stability. As discarded in the conventional MF approaches, tensor-force effects are one of the current hot topics in nuclear structure physics. We investigate effects of the tensor force and those of the spin-isospin channel by comparing the results to those with the Gogny-D1S [16] and D1M [17] interactions.

2 Effective Hamiltonian

Throughout this paper the Hamiltonian is taken to be $H = H_N + V_C - H_{\rm c.m.}$, consisting of the nuclear Hamiltonian H_N, the Coulomb interaction V_C and the center-of-mass (c.m.) Hamiltonian $H_{\rm c.m.}$. The following non-relativistic form is assumed for H_N,

$$H_N = K + V_N\,; \quad K = \sum_i \frac{\mathbf{p}_i^2}{2M}\,, \quad V_N = \sum_{i<j} v_{ij}\,, \tag{1}$$

and

$$\begin{aligned}
v_{ij} &= v_{ij}^{(\rm C)} + v_{ij}^{(\rm LS)} + v_{ij}^{(\rm TN)} + v_{ij}^{(\rm DD)}\,;\\
v_{ij}^{(\rm C)} &= \sum_n \big(t_n^{(\rm SE)} P_{\rm SE} + t_n^{(\rm TE)} P_{\rm TE} + t_n^{(\rm SO)} P_{\rm SO} + t_n^{(\rm TO)} P_{\rm TO}\big) f_n^{(\rm C)}(r_{ij})\,,\\
v_{ij}^{(\rm LS)} &= \sum_n \big(t_n^{(\rm LSE)} P_{\rm TE} + t_n^{(\rm LSO)} P_{\rm TO}\big) f_n^{(\rm LS)}(r_{ij})\, \mathbf{L}_{ij}\cdot(\mathbf{s}_i+\mathbf{s}_j)\,,\\
v_{ij}^{(\rm TN)} &= \sum_n \big(t_n^{(\rm TNE)} P_{\rm TE} + t_n^{(\rm TNO)} P_{\rm TO}\big) f_n^{(\rm TN)}(r_{ij})\, r_{ij}^2 S_{ij}\,,\\
v_{ij}^{(\rm DD)} &= \big(t_\rho^{(\rm SE)} P_{\rm SE}\cdot[\rho(\mathbf{r}_i)]^{\alpha^{(\rm SE)}} + t_\rho^{(\rm TE)} P_{\rm TE}\cdot[\rho(\mathbf{r}_i)]^{\alpha^{(\rm TE)}}\big)\,\delta(\mathbf{r}_{ij})\,,
\end{aligned} \tag{2}$$

where i and j are the indices of individual nucleons, $M = (M_p + M_n)/2$ with M_p (M_n) representing the mass of a proton (a neutron) [18], $\mathbf{s}_i$ is the spin operator of the i-th nucleon, $\mathbf{r}_{ij} = \mathbf{r}_i - \mathbf{r}_j$, $r_{ij} = |\mathbf{r}_{ij}|$, $\mathbf{p}_{ij} = (\mathbf{p}_i - \mathbf{p}_j)/2$, $\mathbf{L}_{ij} = \mathbf{r}_{ij}\times\mathbf{p}_{ij}$, and $\rho(\mathbf{r})$ denotes the nucleon density. The tensor operator is defined by $S_{ij} = 4\,[3(\mathbf{s}_i\cdot\hat{\mathbf{r}}_{ij})(\mathbf{s}_j\cdot\hat{\mathbf{r}}_{ij}) - \mathbf{s}_i\cdot\mathbf{s}_j]$ with $\hat{\mathbf{r}}_{ij} = \mathbf{r}_{ij}/r_{ij}$. The $P_{\rm SE}$, $P_{\rm TE}$, $P_{\rm SO}$ and $P_{\rm TO}$ operators indicate the projection on the singlet-even (SE), triplet-even (TE), singlet-odd (SO) and triplet-odd (TO) two-particle states. The c.m. Hamiltonian is $H_{\rm c.m.} = \mathbf{P}^2/2AM$, where $\mathbf{P} = \sum_i \mathbf{p}_i$ and $A = Z + N$. In the M3Y-type interactions $f_n^{(\rm X)}$ is taken to be the Yukawa function for all of X = C, LS, TN. In the Gogny-D1S and D1M interactions we have $f_n^{(\rm C)}(r) = e^{-(\mu_n r)^2}$, $f^{(\rm LS)}(r) = \nabla^2\delta(\mathbf{r})$ and $v^{(\rm TN)} = 0$. The density-dependent contact term $v^{(\rm DD)}$ carries certain effects of the NNN interaction and the nuclear medium (as introduced via the G-matrix), which are significant to reproduce the saturation properties. It is emphasized that $v^{(\rm TN)}$ is quite realistic in M3Y-P6 and P7, since it is kept unchanged from the M3Y-Paris interaction [19] which has the G-matrix origin. The longest-range part in $v^{(\rm C)}$ is also realistic, maintained to be the corresponding term of the one-pion exchange potential (OPEP) and denoted by $v_{\rm OPEP}^{(\rm C)}$. Owing to $v_{\rm OPEP}^{(\rm C)}$, the M3Y-type interactions have spin-isospin properties consistent with the experimental information [12]. Adjusted to the microscopic results of the pure neutron matter [20, 21], M3Y-P6 and P7 give reasonable symmetry energy up to its density dependence [12].

3 Identification of magic and submagic numbers

Definition of magic numbers is not necessarily clear. Experimentally, they have been identified by relative stability; *e.g.* mass irregularity, kink in the separation energies and high excitation energies. From theoretical viewpoints, the magic nature, which is called "magicity", is linked to quenching of the many-body correlations. Typically, the spherical HF solution is expected to give a good approximation for the doubly magic nuclei. The nuclei having either magic Z or N are usually spherical. For spherical nuclei, the pairing among like nucleons provides dominant correlation beyond the HF. We shall therefore identify magic numbers (and submagic numbers) by comparing the spherical HF and HFB results for even-even nuclei.

The quadrupole deformation can be another source that breaks magicity. However, both the pair excitation and the quadrupole deformation are driven by quenching of the shell gap in most cases, although strength of the residual interaction associated with the individual correlation is relevant as well. Thus the sizable pair correlation within the spherical HFB could also be a measure of the quadrupole deformation. Conversely, when we view breaking of magicity via the pairing in this study, it does not necessarily indicate that the breakdown takes place due to the pair correlation in actual. The present work would give informative overview of distribution of magic numbers over the nuclear chart. Although more precise investigation by taking into account the deformation degrees of freedom (d.o.f) will be desirable, we leave it as a future study which needs intensive calculations.

The magic numbers $Z = 2, 8, 20, 28, 50, 82$ and $N = 2, 8, 20, 28, 50, 82, 126$ have been established around the β stability line. These numbers are kept to be magic in certain region, whereas it has been clarified by experiments that the $N = 8, 20, 28$ magicity is eroded far off the β stability. As will be shown in Sec. 4, $N = 184$ can also be a good magic number, insensitive to Z. We first implement the HF and HFB calculations for even-even nuclei along these numbers. If we find a good candidate for another magic number, we additionally carry out calculations around it. Since validity of the MF approaches could be questioned in very light nuclei and it is difficult to collect experimental data for extremely heavy nuclei, we restrict ourselves to the nuclei having $8 \leq Z \leq 126$ and $N \leq 200$.

From the spherical HFB results, we identify Z (N) to be *magic* when the proton (neutron) pair correlation vanishes. We recognize the vanishing pair correlation through the proton (neutron) pair energy $E_p^{\rm pair}$ ($E_n^{\rm pair}$), *i.e.* the energy contributed by the proton (neutron) pairing tensor in the HFB state. There are certain cases in which the pair correlation survives, but the HF and the HFB energies, which are denoted by $E_{\rm HF}$ and $E_{\rm HFB}$, are very close. In these nuclei correlation effects are suppressed, resulting in *e.g.* relatively high excitation energy. Such suppression takes place particularly when either of Z or N is a good magic number, as has been pointed out for ^{68}Ni [5] and ^{146}Gd [22]. We therefore identify Z (N) to be *submagic* if $E_{\rm HF} - E_{\rm HFB}$ is smaller than a certain value $\lambda_{\rm sub}$ for $N =$ magic ($Z =$ magic) nuclei. We adopt $\lambda_{\rm sub} = 0.5\,{\rm MeV}$ and $0.8\,{\rm MeV}$ in the calculations below, independent of A. Comparison of the results using different $\lambda_{\rm sub}$ values will exhibit how they are sensitive (or insensitive) to $\lambda_{\rm sub}$.

There could be disputes on the above criterion for the magic and submagic numbers. It is true that the criterion based solely on the spherical MF calculations is not complete. We may find influence of quadrupole deformation if comparing the current D1S results to those of the comprehensive deformed HFB calculations [23]. However, previous studies have suggested [5] that the semi-realistic interactions often give simple picture for appearance and disappearance of the magicity, in good connection to the shell structure under the spherical symmetry. Indeed, prediction of magicity with the semi-realistic interactions is in good harmony with the known data, particularly for relatively light-mass region. Moreover, since quadrupole deformation may quench magicity but cannot enhance it, the prediction within the spherical MF regime is useful in selecting candidates and in overviewing how the magic numbers can distribute over the nuclear chart.

There were several works in which the magicity was studied from kinks in the two-proton (S_{2p}) or two-neutron (S_{2n}) separation energies [24]. Whereas S_{2p} and S_{2n} are calculable within the spherical HFB calculations, it is not straightforward to draw a quantitative measure for magicity from S_{2p} and S_{2n} that is applicable to wide range of the nuclear chart. We here comment that the magic and submagic numbers shown below, which are identified from the criterion given above, are compatible with the kinks in the

calculated S_{2p} or S_{2n}.

4 Predicting magic and submagic numbers

We now show prediction on magic and submagic numbers, which are identified by the criterion given in Sec. 3. For the HF and HFB calculations, we have used the methods developed in Ref. [14] with the basis functions of Ref. [15]. The s.p. bases up to $\ell = \ell_{\max} + 2$, where $\ell_{\max}$ is the highest ℓ of the occupied level in the HF configuration, should be included for each nucleus to handle the pair correlation appropriately [14]. We use the $\ell \leq 7$ bases for the $N < 82$ nuclei, the $\ell \leq 8$ bases for the $82 \leq N < 126$ nuclei and the $\ell \leq 9$ bases for the $N \geq 126$ nuclei in the HFB. No additional approximations are imposed, by explicitly treating the exchange and the pairing terms of V_C [25] as well as the 2-body term of $H_{\text{c.m.}}$.

4.1 Overview of magic and submagic numbers

To illustrate how we identify magic and submagic numbers, we show E_n^{pair} and $E_{\text{HF}} - E_{\text{HFB}}$ for the O isotopes calculated with D1M and M3Y-P6, in Fig. 1. Likewise for the $N = 28$ isotones in Fig. 2.

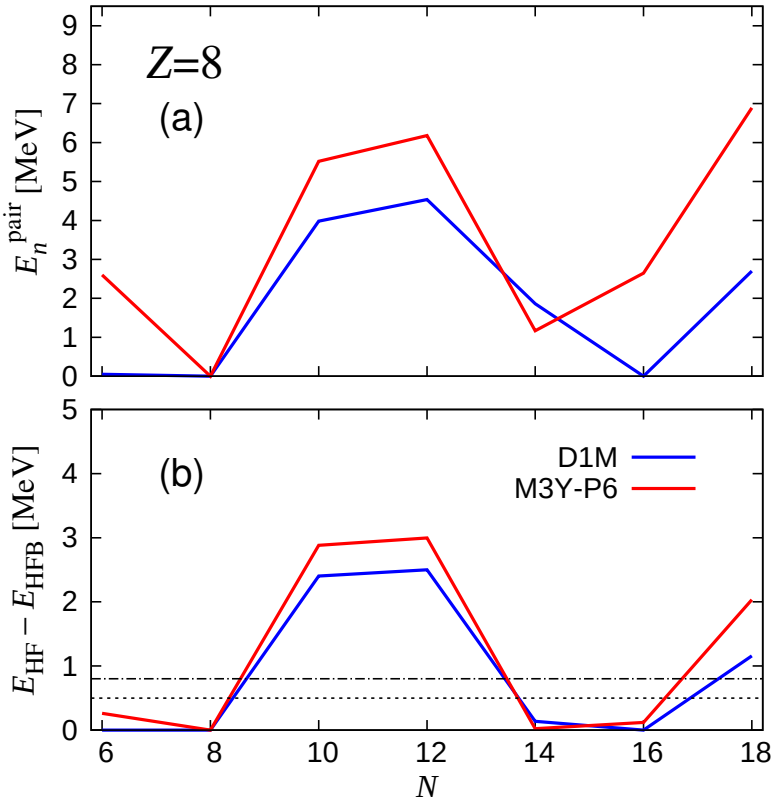

Figure 1: (a) E_n^{pair} and (b) $E_{\text{HF}} - E_{\text{HFB}}$ in the $Z = 8$ nuclei. The blue and red lines present the results with the D1M and M3Y-P6 interactions, respectively. In (b), the λ_{sub} values (0.5 MeV and 0.8 MeV) are shown by the thin dotted and dot-dashed lines.

In the O isotopes we always have $E_p^{\text{pair}} = 0$ and therefore $Z = 8$ is regarded to be magic. Because E_n^{pair} vanishes at $N = 8$, ^{16}O is a good doubly-magic nucleus. We find that E_n^{pair} also vanishes at $N = 16$ with the D1M interaction, indicating that $N = 16$ is a magic number at ^{24}O. With the M3Y-P6 interaction, E_n^{pair} does not fully vanish though relatively small. The suppression of the neutron pairing is confirmed

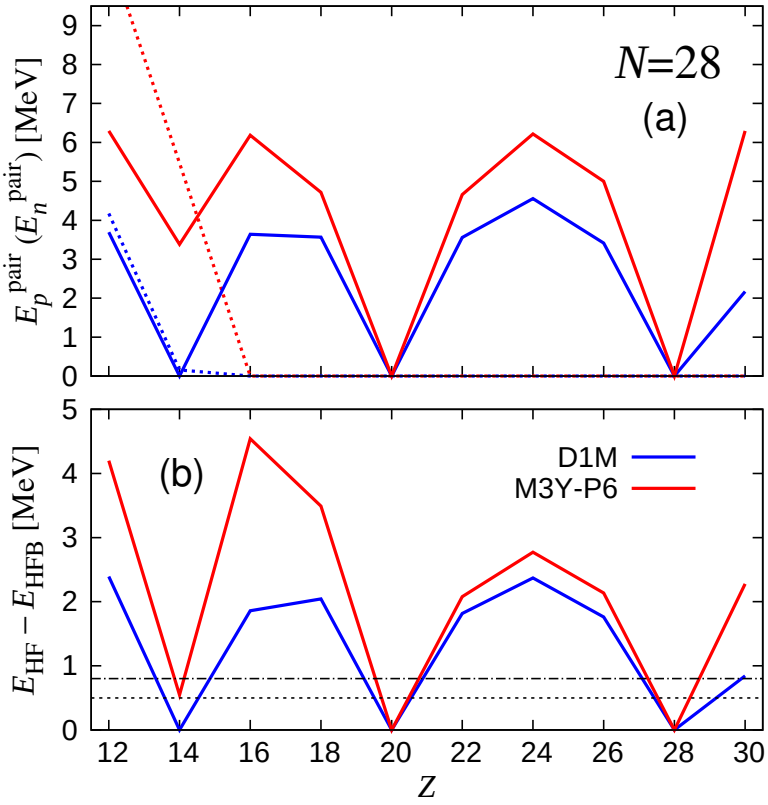

Figure 2: (a) $E_p^{\rm pair}$ ($E_n^{\rm pair}$) and (b) $E_{\rm HF} - E_{\rm HFB}$ in the $N = 28$ nuclei. In (a) $E_n^{\rm pair}$ is presented by the dotted line while $E_p^{\rm pair}$ by the solid lines. Convention of colors is similar to Fig. 1.

in $E_{\rm HF} - E_{\rm HFB}$, and we consider that $N = 16$ is submagic at ^{24}O in the M3Y-P6 result. Analogously, $N = 14$ is submagic both with D1M and M3Y-P6.

In Fig. 2, $E_n^{\rm pair}$ as well as $E_p^{\rm pair}$ are presented for the $N = 28$ isotones. We remark that non-vanishing $E_n^{\rm pair}$ is obtained in the $Z \leq 14$ region with the M3Y-P6 interaction. The same holds with M3Y-P7, though not shown. This well corresponds to the observed breakdown of the $N = 28$ magicity in this region. At ^{42}Si $E_{\rm HF} - E_{\rm HFB}$ is less than 0.8 MeV. However, deformation may be driven because neither Z nor N is magic. For this reason we do not regard $N = 28$ to be submagic at ^{42}Si, although deformed MF calculations are required for full justification. In contrast, when we apply D1M, $Z = 14$ is magic and $N = 28$ remains submagic at ^{42}Si, although the $N = 28$ magicity is lost at ^{40}Mg.

The $N = 28$ magicity holds in $Z \geq 16$. We do not find quenching of the proton pairing in this region, except at the normal magic numbers $Z = 20$ and 28.

We search magic and submagic numbers in this manner in the wide range of the nuclear chart, applying the spherical HF and HFB calculations. The prediction with the M3Y-P6 and P7 semi-realistic interactions is summarized in Figs. 3 and 4. For comparison, the prediction with D1M is displayed in Fig. 5. We shall take a close look at these results, along with the result with D1S, in the subsequent subsections. The boundaries in Figs. 3–5 for the nuclei having magic Z or N are obtained from the spherical HFB calculations. For open-shell nuclei the boundaries are somewhat arbitrary, not representing reliable drip lines, because we have not taken into account deformation in the present work.

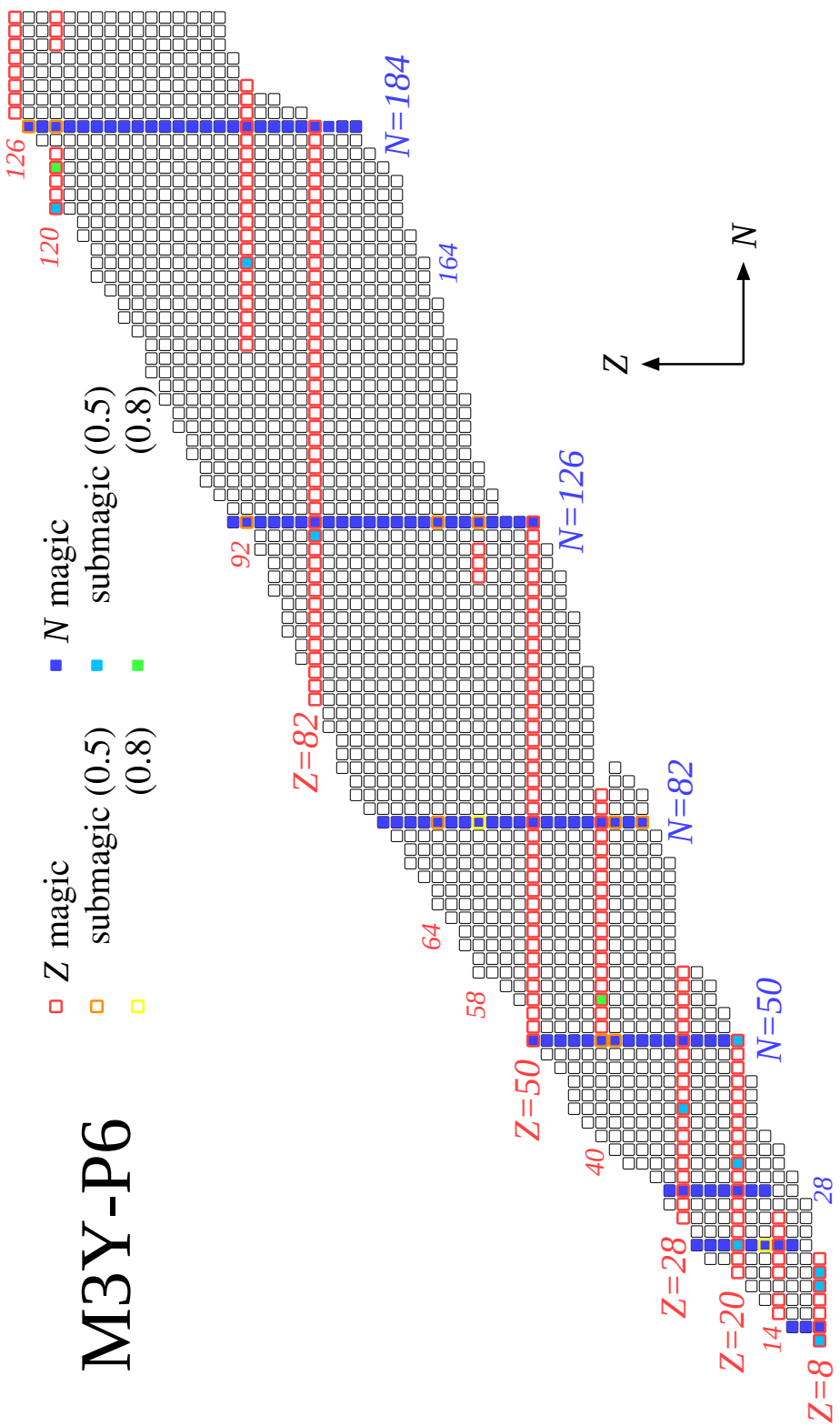

Figure 3: Chart showing magic numbers predicted with the M3Y-P6 interaction. Individual boxes correspond to even-even nuclei. Magic (submagic) Z's are represented by the red-colored (orange- or yellow-colored) frame, and magic (submagic) N's by filling the box with the blue (skyblue or green) color. The $\lambda_{\rm sub}$ values for the submagic numbers (in MeV) are as parenthesized.

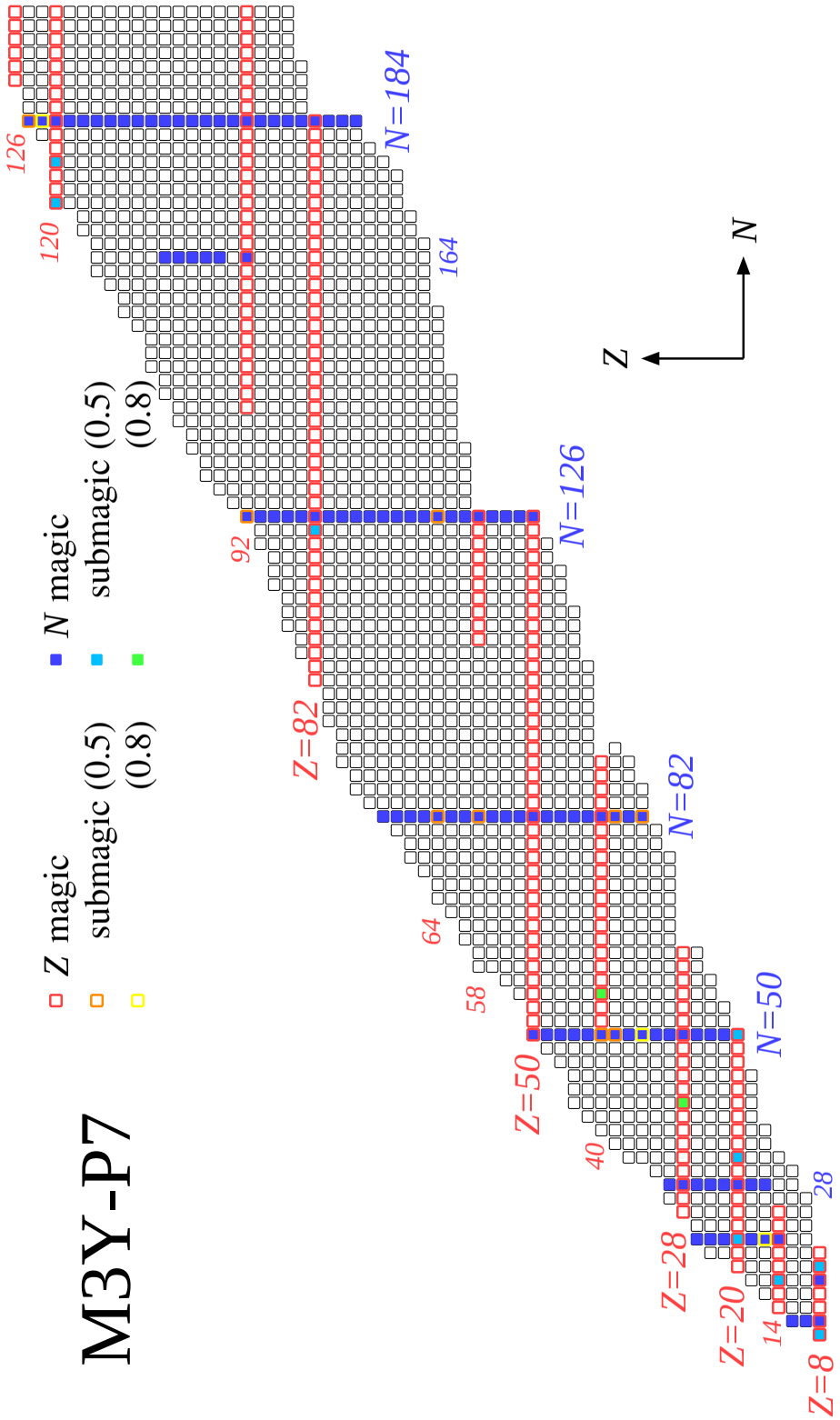

Figure 4: Chart showing magic numbers predicted with the M3Y-P7 interaction. See Fig. 3 for conventions.

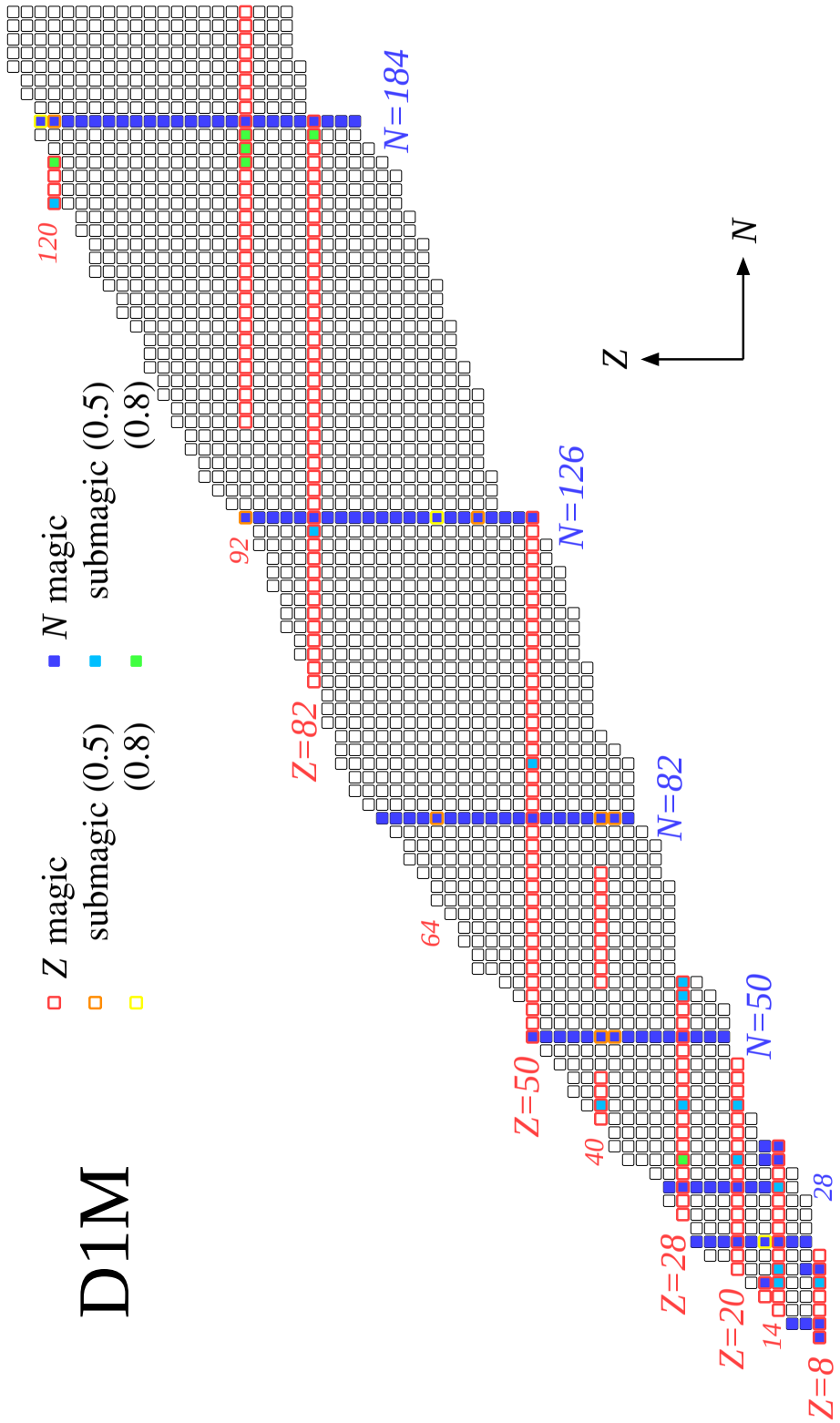

Figure 5: Chart showing magic numbers predicted with the D1M interaction. See Fig. 3 for conventions.

4.2 $N = 6$, 14 and 16

The $N = 16$ magicity at ^{24}O observed in the experiments [3] is more or less reproduced by any of the four interactions; magic in the Gogny interactions (D1S and D1M) while submagic in the M3Y-P6 and P7 interactions. The $N = 16$ magicity is extended to $Z = 10$ with D1M and even to $Z = 14$ with D1S. We find that $N = 14$ as well as $N = 6$ behave magic or submagic in the O nuclei, as seen in Fig. 1.

4.3 $N = 20$ and 28

It is remarked that the $N = 20$ magicity is lost at $Z = 10$ with M3Y-P6 and at $Z = 10, 12$ with M3Y-P7, though not with D1M. This reminds us of the experimentally established 'island of inversion'. Usual interpretation of the island of inversion has been the deformation around $N = 20$ for the $Z \lesssim 12$ nuclei [26], whereas possibility of the large fluctuation of the pairing has also been argued [27]. Although the present calculation does not tell us its mechanism, it is interesting to view that the loss of the magicity is well described with M3Y-P7, and partially with M3Y-P6.

Another notable point is that $N = 20$ becomes submagic at ^{40}Ca, rather than magic, with M3Y-P6 and M3Y-P7. This point should further be investigated in the near future.

As already argued in relation to Fig. 2, the $N = 28$ magicity is lost in $N \leq 14$ in the M3Y-P6 and P7 results, while only in $N \leq 12$ in the D1S and D1M results, although quadrupole deformation has been shown to emerge at ^{42}Si in the deformed HFB calculation with D1S [23].

4.4 $N = 32$, 34 and 40

Although $N = 32$ and 34 are magic for the Si and the S isotopes with D1M (so is $N = 34$ with D1S), this prediction is not supported with the semi-realistic M3Y-P6 and P7 interactions. Irrespective of the interactions, $N = 32$ is submagic at ^{52}Ca owing to the closure of the $n1p_{3/2}$ orbit, as is consistent with the experimental data [28]. However, the $N = 32$ magicity is not found at ^{60}Ni with M3Y-P6 and P7, though kept with D1S and D1M. Origin of the Z- and the interaction-dependence of the $N = 32$ magicity will be discussed in Sec. 5. The recently suggested magicity of $N = 34$ at ^{54}Ca [29] is not seen in Figs. 3 – 5.

The submagic nature of $N = 40$ at ^{68}Ni, which is again compatible with the data [30], is reproduced by all the interactions. On the other hand, the $N = 40$ magicity is lost at ^{60}Ca in the M3Y-P6 and P7 results, while it is preserved in the D1S and D1M results. The $N = 40$ magicity depends on the interactions also at ^{80}Zr, to which we shall return in Sec. 4.10.

4.5 $N = 50$, 56 and 58

We do not find loss of the $N = 50$ magicity except at ^{70}Ca. It is noted that $N = 50$ is indicated to be submagic at ^{70}Ca, rather than magic, with the M3Y-P6 and P7 interactions. The ^{70}Ca nucleus is not bound within the spherical HFB with D1S and D1M.

We find that $N = 56$ is submagic at ^{96}Zr except with D1M because of the $n1d_{5/2}$ closure, well corresponding to the high first excitation energy in the measurements [31]. In the D1S and D1M results $N = 56$ and 58 are submagic in the Ni isotopes. Although the submagic nature of $N = 58$ has been argued using M3Y-P5 in Ref. [5], the magicity is not apparent in the M3Y-P6 and P7 results.

4.6 $N = 82$, 90, 124 and 126

The magicity of $N = 82$ and $N = 126$ is maintained in the whole region of Z.

$N = 90$ is predicted to be submagic with D1S and D1M at ^{140}Sn because the $n1f_{7/2}$ orbit is fully occupied, but not with M3Y-P6 and P7. $N = 124$ becomes submagic at ^{206}Pb with all the interactions, having the $(n2p_{1/2})^{-2}$ configuration.

4.7 $N = 164$, 184 and in-between

$N = 164$ becomes magic with M3Y-P7 at ^{256}U and submagic with M3Y-P6 because of the occupation of the $n0i_{11/2}$, $n1g_{9/2}$ and $n0j_{15/2}$ orbits, while it does not so with the D1S and D1M interactions. The $N = 164$ magicity is developed in the M3Y-P7 results, occurring also in $96 \leq N \leq 104$. The neutron numbers $N = 178$, 180 and 182 are classified to be submagic for the U nuclei with D1M, all of which are not with the M3Y-P6 and P7 interactions. The $N = 178$ magicity is connected to the occupation of $n1g_{7/2}$ and $n2d_{5/2}$, and $N = 182$ is to the additional occupation of $n2d_{3/2}$, leaving $n3s_{1/2}$ unoccupied. However, $N = 180$ is not connected to the subshell closure. The pair correlation seems to come small partly because of the large mass number and the relatively small degeneracy of the relevant orbitals. This problem in the D1M result could be lifted if we introduce A-dependence in $\lambda_{\rm sub}$, though it is not needed for M3Y-P6.

Along $Z = 120$, $N = 172$ and 178 become submagic with all the interactions. With D1S, ^{292}120 is even a doubly magic nucleus and $N = 182$ is also submagic.

$N = 184$ is a good magic number for all the bound nuclei, with any of the interactions employed in the present work, whereas the deformed HFB calculations with D1S have suggested instability against fission in $Z \geq 104$ [23].

4.8 $Z = 14$ and 16

Having $Z = 14$ and $N = 20$, ^{34}Si is predicted to be doubly magic with any of the four interactions, as has been argued in connection to the proton bubble structure [6]. $Z = 14$ stays as a magic number in the results with the D1S and D1M interactions. In contrast, it is not a magic number in $N \geq 26$ with M3Y-P6 and P7, nor at $N = 14$ with M3Y-P6. The stiffness of the $Z = 14$ core seems relevant to where the $N = 28$ magicity is broken, which has been argued in Sec. 4.3.

All the interactions indicate that $Z = 16$ is weakly submagic at ^{36}S. With the D1M interaction $Z = 16$ becomes magic at $N = 12$ and 14 (also at $N = 16$ with D1S), while it is not with the M3Y-P6 and P7 interactions.

4.9 $Z = 20$ and 28

In the present study, $Z = 20$ and 28 remain to be magic numbers in the whole region of N and irrespective of the effective interactions. As pointed out in Ref. [5], the persistence of the $Z = 28$ magicity around ^{78}Ni is contrasted to the argument in Ref. [4], although the realistic tensor force is included in M3Y-P6 and P7. This difference happens because magic numbers are a result of interplay of various interaction channels, even though the tensor force plays a significant role.

4.10 $Z = 34$, 38 and 40

The $Z = 38$ and 40 magicity has been known to be enhanced along the $N = 50$ isotones. This nature is well described, with both Z's staying submagic.

We find that $Z = 34$ is submagic with M3Y-P6 and P7 at $N = 82$ while ^{116}Se is unbound with D1S and D1M. $Z = 38$ is predicted to be submagic with all of the four interactions at ^{120}Sr.

The Zr isotopes have been known to exhibit remarkable N-dependence in their structure. While ^{90}Zr is close to doubly magic, the Zr nuclei are deformed in $60 \leq N \lesssim 70$ as well as in $N \approx 40$. We find that the current results for the Zr isotopes significantly depend on the interactions. Although $Z = 40$ is magic in $38 \leq N \leq 46$ with D1M (in $38 \leq N \leq 48$ with D1S), this magicity is broken with M3Y-P6 and P7, which is consistent with the experimental data. As a typical example, ^{80}Zr is doubly magic with the Gogny interactions, while both Z and N lose magicity with the M3Y-P6 and P7 interactions. The observed energy levels show that ^{80}Zr is deformed and never doubly magic. The deformed HFB does not solve this problem of the D1S interaction [23].

In the present work using the spherical MF calculations, $Z = 40$ is indicated to be magic in $60 \lesssim N \lesssim 70$, with any of the four interactions. This is contradictory to the recent experiments [32]. It is desired

to implement deformed MF calculations, particularly those using the semi-realistic interactions, to check whether and how the experimental data is accounted for.

The ^{122}Zr nucleus is doubly magic in the M3Y-P6 and P7 results, and is close to doubly magic with submagic nature of $Z = 40$ in the Gogny results.

4.11 $Z = 50$, 58 and 64

We predict no breakdown of the $Z = 50$ magicity in the present calculations. However, deformation has been suggested for neutron-rich Sn nuclei in the previous calculations; *e.g.* for $98 \leq N \leq 110$ in the calculations with D1S [23] and similarly in the relativistic MF calculations [33]. Further study is desirable by applying the M3Y-P6 and P7 interactions to the deformed MF calculations.

All the current interactions reproduce the submagic nature of $Z = 64$ at ^{146}Gd, which has long been investigated (*e.g.* Ref. [22]). We also find that $Z = 58$ becomes submagic at ^{140}Ce with M3Y-P6 and P7, though not with D1S and D1M. The measured first excitation energy is slightly higher in ^{140}Ce [34] than in the surrounding $N = 82$ isotones ^{138}Ba and ^{142}Nd.

Irrespective of the interactions, we view certain magicity of $Z = 58$ at ^{184}Ce (magic with M3Y-P7 and submagic with the others), and of $Z = 64$ at ^{190}Gd (submagic with any of the interactions). $Z = 58$ becomes magic in $118 \leq N \leq 122$ with M3Y-P6 and in $108 \leq N \leq 126$ with M3Y-P7, though not in the D1S and D1M results.

4.12 $Z = 82$ and 92

Within the spherical MF calculations, the Pb nuclei are bound up to $N = 184$ with all the interactions, and the last bound nucleus ^{266}Pb is predicted to be a good doubly magic nucleus. Since quadrupole deformation has been predicted to take place in $144 \leq N \leq 166$ by the deformed HFB calculations with D1S [23], stability against deformation should further be investigated in future studies.

The $Z = 92$ number gains certain magicity, behaves as submagic at ^{218}U. Whereas $Z = 92$ is not fully closed in the neutron-deficient region, it is predicted to be magic in $N \gtrsim 150$ in the present work. This magicity is stronger in the D1S, D1M and M3Y-P7 results, even holding at ^{238}U which is a well-known deformed nucleus [35], in contrast to the M3Y-P6 result in which $Z = 92$ is not magic up to $N = 150$. It should be mentioned that deformed ground states have been predicted by the deformed HFB calculations with D1S in $N \lesssim 170$ [23].

4.13 $Z = 120$, 124 and 126

The proton magic numbers beyond $Z = 100$ have attracted interest, in connection to the superheavy nuclei in the so-called 'island of stability'. Although $Z = 114$ has been considered a candidate of a magic number, the present work does not support it irrespectively of the interactions. On the other hand, $Z = 120$ may behave as a magic number. We view that $Z = 120$ is magic in $N \leq 178$ with any of the four interactions. In the M3Y-P7 result the $Z = 120$ magicity extends to $N = 200$, and in the M3Y-P6 result it disappears at $N = 180$ but revives at $N = 196$, apart from its the submagic nature at $N = 184$. The $Z = 120$ magicity is also predicted in $N \leq 182$ and $N \geq 194$ with D1S. In the D1M result the $Z = 120$ magicity is lost in $N \geq 180$, despite its submagic nature at $N = 184$.

$Z = 124$ is predicted to be submagic at $N = 184$ with D1S, M3Y-P6 and P7, while unbound within the spherical HFB with D1M. $Z = 126$ is a good magic number with D1S, M3Y-P6 and M3Y-P7, but not with D1M. It is commented that the fission d.o.f. may enter in the $Z \gtrsim 120$ nuclei [23].

5 Effects of tensor and OPEP-central channels

As mentioned in Sec. 1, the tensor force $v^{(\mathrm{TN})}$ in the NN interaction affects the shell structure to significant degree. The central spin-isospin channel, whose dominant part is $v^{(\mathrm{C})}_{\mathrm{OPEP}}$, may cooperatively contribute to the shell evolution in certain cases [10]. In this section we investigate roles of $v^{(\mathrm{TN})}$ and

$v^{(\mathrm{C})}_{\mathrm{OPEP}}$ in some detail, by analyzing the spherical HF results. Since these channels are explicitly contained in M3Y-P6 and P7 while not in D1S and D1M, comparison among these results will be useful in assessing effects of $v^{(\mathrm{TN})}$ and $v^{(\mathrm{C})}_{\mathrm{OPEP}}$ on the magicity.

We here comment on the difference in the magicity between M3Y-P6 and P7, which is found mainly in heavier mass region in Figs. 3 and 4. As the $v^{(\mathrm{TN})}$ and $v^{(\mathrm{C})}_{\mathrm{OPEP}}$ channels are identical between them, it is not obvious what is the main source of the difference between M3Y-P6 and P7. Although these two parameter-sets yield different neutron-matter energies at high densities, it is not likely that this significantly influences the magicity of nuclei. The strength of $v^{(\mathrm{LS})}$, which is slightly stronger in M3Y-P7 than in M3Y-P6, does not account for all the visible difference between Figs. 3 and 4.

The s.p. energy of the orbit j, $\varepsilon_{\tau_z}(j)$ ($\tau_z = p, n$), is defined by the derivative of the total energy with respect to the occupation probability. We extract contribution of $v^{(\mathrm{TN})}$ to $\varepsilon_{\tau_z}(j)$ from the full HF result by

$$\varepsilon^{(\mathrm{TN})}_{\tau_z}(j) = \sum_{j'm'} n_{j'} \langle jmj'm'|v^{(\mathrm{TN})}|jmj'm'\rangle = \frac{1}{2j+1}\sum_{j'J} n_{j'}(2J+1)\langle jj'J|v^{(\mathrm{TN})}|jj'J\rangle\,, \tag{3}$$

where n_j denotes the occupation probability on j. Likewise for $\varepsilon^{(\mathrm{OPEP})}_{\tau_z}(j)$, *i.e.* contribution of $v^{(\mathrm{C})}_{\mathrm{OPEP}}$. For the shell gap $\Delta\varepsilon_{\tau_z}(j_2\text{-}j_1) = \varepsilon_{\tau_z}(j_2) - \varepsilon_{\tau_z}(j_1)$, corresponding quantities $\Delta\varepsilon^{(\mathrm{TN})}_{\tau_z}(j_2\text{-}j_1)$ and $\Delta\varepsilon^{(\mathrm{OPEP})}_{\tau_z}(j_2\text{-}j_1)$ can be considered. Since the s.p. energies are more or less fitted to the data in each effective interaction, the absolute values of $\Delta\varepsilon^{(\mathrm{TN})}_{\tau_z}(j_2\text{-}j_1)$ or $\Delta\varepsilon^{(\mathrm{OPEP})}_{\tau_z}(j_2\text{-}j_1)$ are not very meaningful. However, Z- or N-dependence of $\Delta\varepsilon^{(\mathrm{TN})}_{\tau_z}(j_2\text{-}j_1)$ and $\Delta\varepsilon^{(\mathrm{OPEP})}_{\tau_z}(j_2\text{-}j_1)$ is important, which may give rise to the Z- or N-dependence of the shell gap. We shall argue several typical cases in which $v^{(\mathrm{TN})}$ and/or $v^{(\mathrm{C})}_{\mathrm{OPEP}}$ play a significant role in Z- or N-dependence of the magicity.

5.1 $N = 16$, 32 and 40

While $N = 16$ behaves as magic or submagic at ^{24}O irrespectively of the effective interactions, its magicity depends on the interactions for larger Z, *i.e.* near the β stability. The shell gap $\Delta\varepsilon_n(0d_{3/2} - 1s_{1/2})$ is relevant to the $N = 16$ magicity. In Ref. [10] we have shown that $v^{(\mathrm{TN})}$ and $v^{(\mathrm{C})}_{\mathrm{OPEP}}$ give the Z-dependence by using the older parameter-set M3Y-P5. Analogous results are obtained with the present parameters M3Y-P6 and P7, which we do not repeat here.

The $N = 32$ magicity is basically determined by $\Delta\varepsilon_n(0f_{5/2}\text{-}1p_{3/2})$ or $\Delta\varepsilon_n(1p_{1/2}\text{-}1p_{3/2})$. As mentioned in Sec. 4, $N = 32$ is submagic at ^{52}Ca but not at ^{60}Ni with the M3Y-P6 and P7 interactions. We have found that $N = 40$ is submagic at ^{68}Ni but not at ^{60}Ca in the M3Y results, though submagic at both nuclei in the Gogny results. The highest occupied neutron orbit is $1p_{1/2}$ at ^{68}Ni while $0f_{5/2}$ at ^{60}Ca. The strong Z-dependence of $\Delta\varepsilon_n(0g_{9/2}\text{-}0f_{5/2})$ due to $v^{(\mathrm{TN})}$ is important to the erosion of the $N = 40$ magicity at ^{60}Ca. Role of $v^{(\mathrm{TN})}$ and $v^{(\mathrm{C})}_{\mathrm{OPEP}}$ in the $N = 32$ and 40 magicity was already presented in Ref. [5] by employing M3Y-P5. Essential points do not change with M3Y-P6 and P7.

5.2 $N = 56$

From Figs. 3 – 5 we have found that the submagic nature of $N = 56$ at ^{96}Zr is well accounted for with M3Y-P6 and P7, but not with D1S and D1M. We present the relevant s.p. energy difference $\Delta\varepsilon_n(0g_{7/2}\text{-}1d_{5/2})$ in Fig. 6, for D1M and M3Y-P6. It is found that $\Delta\varepsilon_n$ strongly depends on Z in the M3Y-P6 result, as $p0g_{9/2}$ is occupied in $40 \le Z \le 50$. This Z-dependence produces the relatively large gap at ^{96}Zr. The M3Y-P6 result also suggests that $n1d_{5/2}$ and $n0g_{7/2}$ are nearly degenerate around ^{106}Sn, compatible with the observed levels in ^{105,107}Sn [36].

In order to clarify effects of $v^{(\mathrm{C})}_{\mathrm{OPEP}}$ and $v^{(\mathrm{TN})}$ on the Z-dependence of the shell gap, $\Delta\varepsilon_n - \Delta\varepsilon^{(\mathrm{OPEP})}_n$ is plotted by the thin red dotted line and $\Delta\varepsilon_n - \Delta\varepsilon^{(\mathrm{OPEP})}_n - \Delta\varepsilon^{(\mathrm{TN})}_n$ by the thin red dot-dashed line in Fig. 6. The difference between the red solid line and the red dotted line corresponds to $\Delta\varepsilon^{(\mathrm{OPEP})}_n(0g_{7/2}\text{-}1d_{5/2})$, representing effects of $v^{(\mathrm{C})}_{\mathrm{OPEP}}$, and the difference between the red dotted line and the red dot-dashed line

to $\Delta\varepsilon_n^{(\mathrm{TN})}(0g_{7/2}\text{-}1d_{5/2})$, showing effects of $v^{(\mathrm{TN})}$. It is found that the difference in the s.p. energies depends on Z only weakly as long as we do not have contributions of $v_{\mathrm{OPEP}}^{(\mathrm{C})}$ and $v^{(\mathrm{TN})}$, both from the D1M result and the M3Y-P6 result of $\Delta\varepsilon_n - \Delta\varepsilon_n^{(\mathrm{OPEP})} - \Delta\varepsilon_n^{(\mathrm{TN})}$. It is reasonable to conclude that $v^{(\mathrm{TN})}$ and $v_{\mathrm{OPEP}}^{(\mathrm{C})}$ are responsible for the Z-dependence.

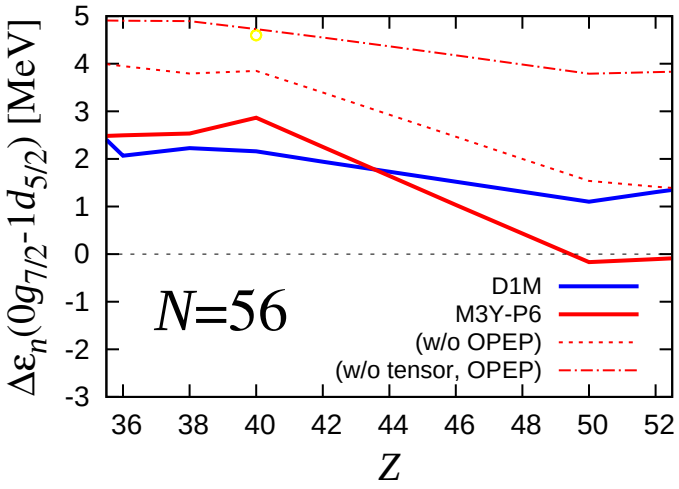

Figure 6: $\Delta\varepsilon_n(0g_{7/2}\text{-}1d_{5/2})$ in the $N = 56$ nuclei. Blue and red solid lines are the results with D1M and M3Y-P6, respectively. The yellow circle at the top part of the figure indicates that $N = 56$ is submagic at $Z = 40$ in Fig. 3 (*i.e.* the M3Y-P6 result). Thin red dotted and dot-dashed lines are obtained by subtracting contributions of $v^{(\mathrm{TN})}$ and $v_{\mathrm{OPEP}}^{(\mathrm{C})}$ from the M3Y-P6 result; see text for details.

5.3 $N = 164$

As shown in Figs. 3–5 $N = 164$ becomes a submagic with M3Y-P6 and a magic number with M3Y-P7 at ^{256}U, although it is not with the D1S and D1M interactions. The $N = 164$ shell gap is primarily determined by $\Delta\varepsilon_n(1g_{7/2}\text{-}0j_{15/2})$, and is relevant also to $\Delta\varepsilon_n(2d_{5/2}\text{-}0j_{15/2})$. These s.p. energy differences are shown for D1M and M3Y-P6 in Fig. 7. We find enhancement of the gap at $Z = 92$ in the M3Y-P6 case, which is regarded as origin of the magicity. We do not have similar Z-dependence in the D1M result.

For $\Delta\varepsilon_n(1g_{7/2}\text{-}0j_{15/2})$, the M3Y-P6 result of $\Delta\varepsilon_n - \Delta\varepsilon_n^{(\mathrm{OPEP})}$ (the thin red dotted line) and $\Delta\varepsilon_n - \Delta\varepsilon_n^{(\mathrm{OPEP})} - \Delta\varepsilon_n^{(\mathrm{TN})}$ (the thin red dot-dashed line) is plotted in Fig. 7. We find that $\Delta\varepsilon_n(1g_{7/2}\text{-}0j_{15/2})$ is insensitive to Z in the D1M result and in the M3Y-P6 result after subtracting the contributions of $v_{\mathrm{OPEP}}^{(\mathrm{C})}$ and $v^{(\mathrm{TN})}$. It is thus clarified that the $N = 164$ magicity emerges primarily by $v^{(\mathrm{TN})}$ and complementarily by $v_{\mathrm{OPEP}}^{(\mathrm{C})}$.

5.4 $Z = 14$

We have shown in Figs. 3–5 that $Z = 14$ behaves as a good magic number for all N with D1M, while its magicity depends on N with M3Y-P6 and P7. The relevant s.p. energy differences $\Delta\varepsilon_p(1s_{1/2}\text{-}0d_{5/2})$ and $\Delta\varepsilon_p(0d_{3/2}\text{-}0d_{5/2})$ are presented in Fig. 8 for D1M and M3Y-P6. It is noted that, while $n0d_{3/2}$ is higher than $n1s_{1/2}$ for all N in the D1M result, $n0d_{3/2}$ comes down so that the level sequence could be inverted in $N \geq 26$ in the M3Y-P6 result. The breakdown of the $Z = 14$ magicity at $N \approx 28$ with M3Y-P6 seems linked to this behavior of $n0d_{3/2}$.

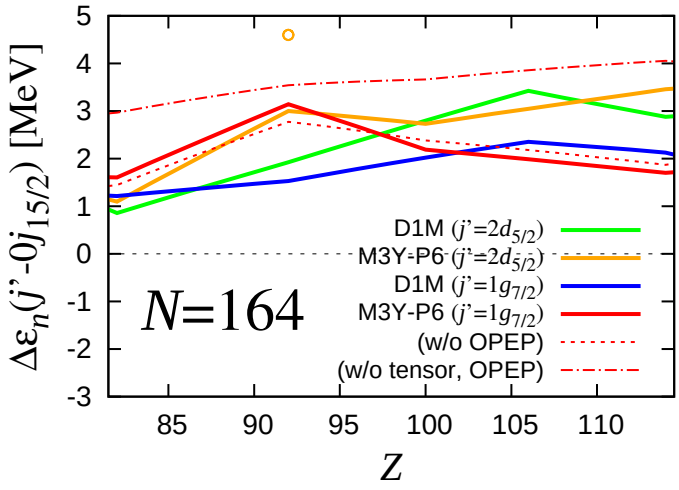

Figure 7: $\Delta\varepsilon_n(j'\text{-}0j_{15/2})$ ($j' = 2d_{5/2}$ or $1g_{7/2}$) in the $N = 164$ nuclei. Green (orange) solid line is for $j' = 2d_{5/2}$ calculated with D1M (M3Y-P6), and blue (red) solid line is for $j' = 1g_{7/2}$ with D1M (M3Y-P6). $N = 164$ is submagic at $Z = 92$ in Fig. 3, which is indicated by the orange circle at the top part of the figure. We have no other magicity in Figs. 3 and 5 (*i.e.* the D1M result). Thin red dotted and dot-dashed lines are obtained by subtracting contributions of $v^{(\mathrm{TN})}$ and $v^{(\mathrm{C})}_{\mathrm{OPEP}}$ in $\Delta\varepsilon_n(1g_{7/2}\text{-}0j_{15/2})$ with M3Y-P6, as in Fig. 6.

Effects of $v^{(\mathrm{C})}_{\mathrm{OPEP}}$ and $v^{(\mathrm{TN})}$ on $\Delta\varepsilon_p(0d_{3/2}\text{-}0d_{5/2})$ are investigated by plotting $\Delta\varepsilon_p - \Delta\varepsilon_p^{(\mathrm{OPEP})}$ (the thin red dotted line) and $\Delta\varepsilon_p - \Delta\varepsilon_p^{(\mathrm{OPEP})} - \Delta\varepsilon_p^{(\mathrm{TN})}$ (the thin red dot-dashed line) in Fig. 8. After contributions of $v^{(\mathrm{C})}_{\mathrm{OPEP}}$ and $v^{(\mathrm{TN})}$ are subtracted, $\Delta\varepsilon_p(0d_{3/2}\text{-}0d_{5/2})$ with M3Y-P6 does not have strong N-dependence in $20 \le N \le 28$, becoming almost parallel to the corresponding D1M result. Such similarity in the slope has been seen in the Ca isotopes in Ref. [6]. We confirm that the strong N-dependence of $\Delta\varepsilon_p(0d_{3/2}\text{-}0d_{5/2})$ from $N = 20$ to 28 predominantly originates in $v^{(\mathrm{TN})}$, aided by subsidiary contribution of $v^{(\mathrm{C})}_{\mathrm{OPEP}}$.

5.5 $Z = 40$

The s.p. energy difference relevant to the $Z = 40$ magicity is $\Delta\varepsilon_p(0g_{9/2}\text{-}1p_{1/2})$. We compare N-dependence of $\Delta\varepsilon_p(0g_{9/2}\text{-}1p_{1/2})$ between D1M and M3Y-P6 in Fig. 9.

We find opposite trends between the D1M and the M3Y-P6 results on $\Delta\varepsilon_p(0g_{9/2}\text{-}1p_{1/2})$ in $40 \le N \le 50$ as $n0g_{9/2}$ is occupied, and in $70 \le N \le 82$ as $n0h_{11/2}$ is occupied. In addition, the rising tendency of $\Delta\varepsilon_p(0g_{9/2}\text{-}1p_{1/2})$ at $N \approx 60$ in the M3Y-P6 result is not conspicuous with D1M. It is notable that, after contributions of $v^{(\mathrm{C})}_{\mathrm{OPEP}}$ and $v^{(\mathrm{TN})}$ are subtracted, the M3Y-P6 result becomes almost parallel to that of D1M. On the contrary, once $v^{(\mathrm{TN})}$ is set in, the s.p. energy difference has quite similar N-dependence to the full result. This clarifies significance of $v^{(\mathrm{TN})}$ in the N-dependence of the shell gap at $Z = 40$. Relatively small $\Delta\varepsilon_p(0g_{9/2}\text{-}1p_{1/2})$ at $N = 40$ contributes to the loss of the $Z = 40$ magicity around ^{80}Zr viewed in Fig. 3, and relatively large $\Delta\varepsilon_p(0g_{9/2}\text{-}1p_{1/2})$ at $N = 82$ to the persistence of the magicity around ^{122}Zr. The large $\Delta\varepsilon_p(0g_{9/2}\text{-}1p_{1/2})$ at $N \approx 60$ prevents the $Z = 40$ magicity from being broken within the spherical HFB. It will be an interesting future subject whether and how the observed deformation at $N \gtrsim 60$ is accounted for, under the sizable shell gap brought by $v^{(\mathrm{TN})}$.

5.6 $Z = 58$

The $Z = 58$ magicity in the neutron-rich region of $N \gtrsim 110$ takes place because of the $p0g_{7/2}$ occupation, to which the energy difference $\Delta\varepsilon_p(1d_{5/2}\text{-}0g_{7/2})$ is relevant. However, when comparing $\Delta\varepsilon_p(1d_{5/2}\text{-}0g_{7/2})$

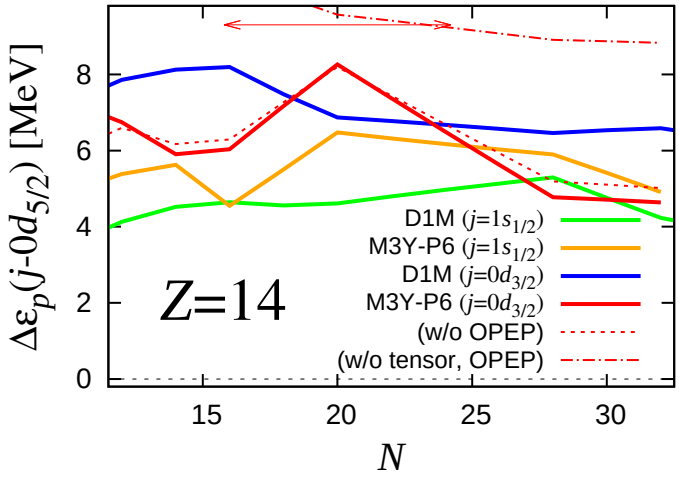

Figure 8: $\Delta\varepsilon_p(j\text{-}0d_{5/2})$ ($j = 1s_{1/2}$ or $0d_{3/2}$) in the $Z = 14$ nuclei. Green (orange) solid line is for $j = 1s_{1/2}$ calculated with D1M (M3Y-P6), and blue (red) solid line is for $j = 0d_{3/2}$ with D1M (M3Y-P6). The region where $Z = 14$ is magic in Fig. 3 is shown by the red arrow at the top part of the figure, while in Fig. 5 $Z = 14$ is magic for all N. $\Delta\varepsilon_p(0d_{3/2}\text{-}0d_{5/2})$'s after subtracting the $v^{(\mathrm{TN})}$ and $v^{(\mathrm{C})}_{\mathrm{OPEP}}$ contributions from the M3Y-P6 result are displayed by thin red dotted and dot-dashed lines, as in Fig. 6.

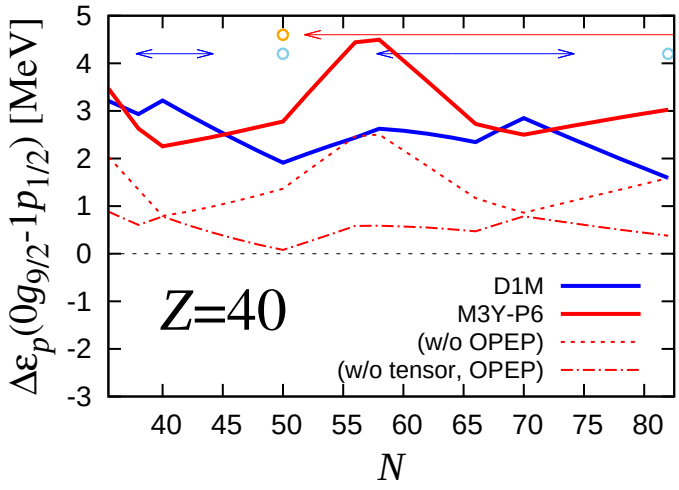

Figure 9: $\Delta\varepsilon_p(0g_{9/2}\text{-}1p_{1/2})$ in the $Z = 40$ nuclei. Blue and red solid lines are the results with D1M and M3Y-P6, respectively. For the latter, thin red dotted and dot-dashed lines represent effects of $v^{(\mathrm{TN})}$ and $v^{(\mathrm{C})}_{\mathrm{OPEP}}$ as in Fig. 6. The region where $Z = 40$ is magic in Fig. 5 (Fig. 3) is shown by the blue (red) arrows, and submagic by the skyblue (orange) circles at the top part of the figure.

between D1M and M3Y-P6, it should be noted that $n0i_{13/2}$ lies lower than $n2p_{3/2}$ in the spherical HF calculation with M3Y-P6 in $100 \le N \le 120$, while these two orbits are inverted with D1M except at ^{172}Ce. We therefore show $\Delta\varepsilon_p(1d_{5/2}\text{-}0g_{7/2})$ with D1M in which the s.p. levels were filled in the same ordering as in the M3Y-P6 case, by the blue dashed line in Fig. 10. If the neutron occupation is taken to be similar, $\Delta\varepsilon_p(1d_{5/2}\text{-}0g_{7/2})$ with M3Y-P6 after removing the $v^{(\mathrm{C})}_{\mathrm{OPEP}}$ and $v^{(\mathrm{TN})}$ contributions is almost parallel to $\Delta\varepsilon_p(1d_{5/2}\text{-}0g_{7/2})$ with D1M. As seen in Fig. 10, $v^{(\mathrm{TN})}$ gives rise to large $\Delta\varepsilon_p(1d_{5/2}\text{-}0g_{7/2})$

at $N \approx 114$, with a cooperative effect of $v^{(\mathrm{C})}_{\mathrm{OPEP}}$. Although its degree depends on other channels of the interactions as recognized by comparing Figs. 3 and 4, it is expected that the $Z = 58$ magicity is enhanced in $N \gtrsim 110$ because of $v^{(\mathrm{TN})}$ and $v^{(\mathrm{C})}_{\mathrm{OPEP}}$.

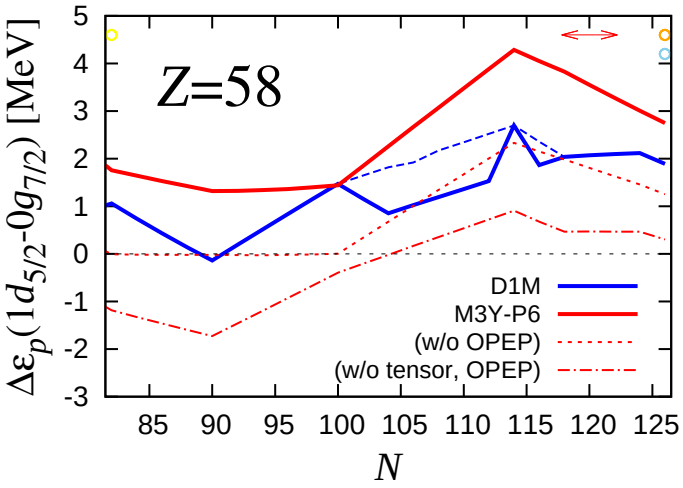

Figure 10: $\Delta\varepsilon_p(1d_{5/2}\text{-}0g_{7/2})$ in the $Z = 58$ nuclei. The blue dashed line is obtained with D1M by filling the s.p. levels in the same order as in the M3Y-P6 result. The red arrow, orange and yellow circles at the top of the figure correspond to the magic and submagic numbers in Fig. 3, while the skyblue circle to the submagic number in Fig. 5. See Fig. 6 for other conventions.

5.7 Assessment of tensor force and OPEP effects

To quantify the Z- or N-dependence of the shell gap, we consider double difference of the s.p. energies $\delta\Delta\varepsilon_{\tau_z}(j_2\text{-}j_1)$ ($\tau_z = p, n$): $\Delta\varepsilon_{\tau_z}(j_2\text{-}j_1)$ at a certain nuclide (Z_2, N_2) relative to that at a reference nuclide (Z_1, N_1). The reference nuclides are chosen so that they should be relatively close to the β-stability line. We can then view the effects of $v^{(\mathrm{TN})}$ and $v^{(\mathrm{C})}_{\mathrm{OPEP}}$ on $\delta\Delta\varepsilon_{\tau_z}(j_2\text{-}j_1)$ through the corresponding quantities $\delta\Delta\varepsilon^{(\mathrm{TN})}_{\tau_z}(j_2\text{-}j_1)$ and $\delta\Delta\varepsilon^{(\mathrm{OPEP})}_{\tau_z}(j_2\text{-}j_1)$. Figure 11 summarizes the effects of $v^{(\mathrm{TN})}$ and $v^{(\mathrm{C})}_{\mathrm{OPEP}}$ on $\delta\Delta\varepsilon_{\tau_z}(j_2\text{-}j_1)$ in the HF results with the M3Y-P6 interaction, by selecting the nuclei at which $v^{(\mathrm{TN})}$ affects the magic numbers. We find that $\delta\Delta\varepsilon^{(\mathrm{OPEP})}_{\tau_z}(j_2\text{-}j_1)$ usually has equal sign but does not exceed $\delta\Delta\varepsilon^{(\mathrm{TN})}_{\tau_z}(j_2\text{-}j_1)$ as long as sizable, although it should not be discarded in many cases.

We look at some of the individual results in Fig. 11 for illustration. The $\Delta\varepsilon_n(0d_{3/2}\text{-}1s_{1/2})$ value at ^{24}O relative to that at ^{30}Si is shown at the top row of Fig. 11. This seems to account for the $N = 16$ magicity at ^{24}O. We obtain $\delta\Delta\varepsilon_n(0d_{3/2}\text{-}1s_{1/2}) = 2.9\,\mathrm{MeV}$ with M3Y-P6, which means that the $N = 16$ shell gap is larger at ^{24}O than at ^{30}Si by 2.9 MeV. Since $\delta\Delta\varepsilon^{(\mathrm{TN})}_n(0d_{3/2}\text{-}1s_{1/2}) = 2.0\,\mathrm{MeV}$ and $\delta\Delta\varepsilon^{(\mathrm{OPEP})}_n(0d_{3/2}\text{-}1s_{1/2}) = 1.3\,\mathrm{MeV}$, it is difficult to obtain the enhancement of the shell gap without $v^{(\mathrm{TN})}$ and $v^{(\mathrm{C})}_{\mathrm{OPEP}}$. The gap could even be reduced from ^{30}Si to ^{24}O without them.

At the second top row of Fig. 11, $\delta\Delta\varepsilon_n(1p_{3/2}\text{-}0f_{7/2})$ obtained as $\Delta\varepsilon_n(1p_{3/2}\text{-}0f_{7/2})$ at ^{42}Si relative to that at ^{48}Ca is presented. The negative value of $\delta\Delta\varepsilon_n(1p_{3/2}\text{-}0f_{7/2})$ indicates quenching of the $N = 28$ shell gap at ^{42}Si. However, $v^{(\mathrm{TN})}$ gives only -0.6 MeV to the full $\delta\Delta\varepsilon_n(1p_{3/2}\text{-}0f_{7/2})$ ($= -2.9$ MeV), and $v^{(\mathrm{C})}_{\mathrm{OPEP}}$ contribution is small but positive (not visible in Fig. 11). Though the $v^{(\mathrm{TN})}$ effect should not be ignored in describing the $N = 28$ shell erosion, it is not necessarily dominant.

We next discuss $\delta\Delta\varepsilon_p(0g_{9/2}\text{-}1p_{1/2})$ evaluated for ^{80}Zr relative to ^{90}Zr. We have -0.5 MeV in the full M3Y-P6 result, while $\delta\Delta\varepsilon^{(\mathrm{TN})}_p(0g_{9/2}\text{-}1p_{1/2}) = -1.3\,\mathrm{MeV}$. Namely, the sign of $\delta\Delta\varepsilon_p(0g_{9/2}\text{-}1p_{1/2})$ is

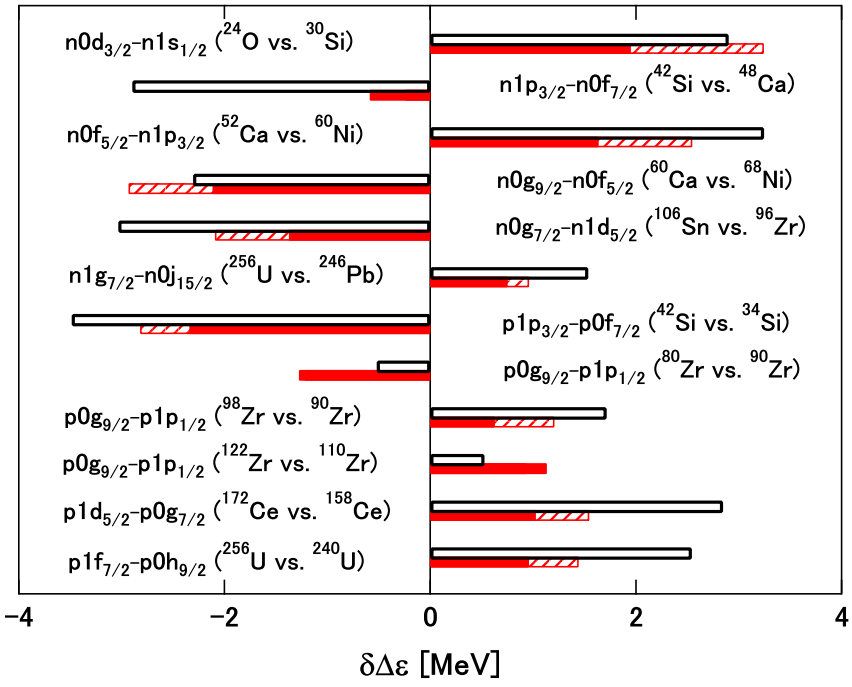

Figure 11: Difference of the shell gaps between two members of isotopes or isotones $\delta\Delta\varepsilon_{\tau_z}(j_2\text{-}j_1)$ (open bars), with contributions of $v^{(\mathrm{TN})}$ (red filled bars) and $v^{(\mathrm{C})}_{\mathrm{OPEP}}$ (red hatched bars) to it, obtained from the HF results with M3Y-P6. See text for details.

inverted owing to $v^{(\mathrm{TN})}$, which could be crucial in the erosion of the $Z = 40$ magicity at $N \approx 40$. Sign inversion due to $v^{(\mathrm{TN})}$ is found also in the comparison between ^{122}Zr and ^{110}Zr, which could be important to persistence of the $N = 82$ magicity around ^{122}Zr.

Several points on the tensor-force and OPEP effects are confirmed from Fig. 11:

- The tensor force often plays a significant role in the Z- or N-dependence of the shell gap, accounting for appearance and disappearance of magicity.
- The central spin-isospin channel from the OPEP tends to enhance the tensor-force effect. Strong Z- or N-dependence of the shell gap often coincides with their cooperative contribution.
- These effects strongly appear as an orbit with relatively high ℓ is occupied.

6 Conclusion

We predict magic and submagic numbers in wide range of the nuclear chart from the spherical mean-field calculations with the M3Y-P6 and P7 semi-realistic NN interactions, which contain the tensor force from the G-matrix as well as the central spin-isospin channel from the OPEP. The magic numbers are identified by vanishing pair correlations in the HFB results, and the submagic numbers by small difference between the HFB and the HF energies. Although deformation degrees of freedom are not explicitly taken into account, the semi-realistic interactions describe the erosion of the $N = 20$ and 28 magicity in the proton-deficient region, as well as the emergence of the $N = 16$ and 32 magicity. In addition to the known magic numbers, possible magicity at $N = 40$, 56, 90, 124, 172, 178, 164, 184 and $Z = 14$, 16, 34, 38, 40, 58, 64, 92, 120, 124, 126 has been argued, in comparison with similar prediction obtained with the Gogny D1S and D1M interactions. The predictions with M3Y-P6 do not contradict to the known data

apparently, except at ^{32}Mg and the Zr isotopes with $60 \leq N \lesssim 70$. Although calculations including the deformation degrees of freedom are needed for complete understanding of the magic numbers, this work will be useful in selecting candidates of the magic numbers and in overviewing how the magic numbers can distribute over the nuclear chart.

By analyzing the shell gaps, roles of the tensor force and of the central spin-isospin channel from the OPEP are investigated. It is confirmed that the tensor force often plays a significant role in the Z- or N-dependence of the shall gap, accounting for appearance and disappearance of magicity, and the central spin-isospin channel tends to enhance the tensor-force effect for emergence of the magicity. The present results are qualitatively consistent with Refs. [4, 7], although quantitative aspects should not be underestimated because they make difference in certain cases.

It will be interesting to study effects of deformation on the magicity with the semi-realistic interactions, and to investigate whether and how the discrepancy between the current results and the data in several nuclei could be resolved.

Acknowledgment

The authors are grateful to T. Inakura for discussions and his assistance in drawing the figures. This work is financially supported as Grant-in-Aid for Scientific Research (C), Nos. 22540266 and 25400245, by Japan Society for the Promotion of Science, and as Grant-in-Aid for Scientific Research on Innovative Areas, No. 24105008, by The Ministry of Education, Culture, Sports, Science and Technology, Japan. Numerical calculations are performed on HITAC SR16000s at Institute of Management and Information Technologies in Chiba University, at Yukawa Institute for Theoretical Physics in Kyoto University, at Information Technology Center in University of Tokyo, and at Information Initiative Center in Hokkaido University.

References

[1] O. Sorlin and M.-G. Porquet, Prog. Part. Nucl. Phys. **61**, 602 (2008).

[2] T. Otsuka, Eur. Phys. J ST **156**, 169 (2008).

[3] A. Ozawa *et al.*, Phys. Rev. Lett. **84**, 5493 (2000).

[4] T. Otsuka, T. Suzuki, R. Fujimoto, H. Grawe and Y. Akaishi, Phys. Rev. Lett. **95**, 232502 (2005).

[5] H. Nakada, Phys. Rev. C **81**, 051302(R) (2010).

[6] H. Nakada, K. Sugiura and J. Margueron, Phys. Rev. C **87**, 067305 (2013).

[7] T. Otsuka *et al.* Phys. Rev. Lett. **87**, 082502 (2001).

[8] T. Otsuka, T. Suzuki, J.D. Holt, A. Schwenk and Y. Akaishi, Phys. Rev. Lett. **105**, 032501 (2010)

[9] H. Nakada, Phys. Rev. C **68**, 014316 (2003).

[10] H. Nakada, Phys. Rev. C **78**, 054301 (2008); *ibid.* **82**, 029902(E) (2010).

[11] H. Nakada, Phys. Rev. C **81**, 027301 (2010); *ibid.* **82**, 029903(E) (2010).

[12] H. Nakada, Phys. Rev. C **87**, 014336 (2013).

[13] H. Nakada and M. Sato, Nucl. Phys. A **699**, 511 (2002); *ibid.* **714**, 696 (2003).

[14] H. Nakada, Nucl. Phys. A **764**, 117 (2006); *ibid.* **801**, 169 (2008).

[15] H. Nakada, Nucl. Phys. A **808**, 47 (2008).

[16] J.F. Berger, M. Girod and D. Gogny, Comp. Phys. Comm. **63**, 365 (1991).

[17] S. Goriely, S. Hilaire, M. Girod and S. Pèru, Phys. Rev. Lett. **102**, 242501 (2009).

[18] W.-M. Yao *et al.* (ParticleDataGroup), J. Phys. G **33**, 1 (2006).

[19] N. Anantaraman, H. Toki and G.F. Bertsch, Nucl. Phys. A **398**, 269 (1983).

[20] B. Friedman and V.R. Pandharipande, Nucl. Phys. A **361**, 502 (1981).

[21] A. Akmal, V.R. Pandharipande and D.G. Ravenhall, Phys. Rev. C **58**, 1804 (1998).

[22] T. Matsuzawa, H. Nakada, K. Ogawa and G. Momoki, Phys. Rev. C **62**, 054304 (2000); *ibid.* **63**, 029902(E) (2001).

[23] S. Hilaire and M. Girod, http://www-phynu.cea.fr/science_en_ligne/carte_potentiels_microscopiques/carte_potentiel_nucleaire_eng.htm.

[24] C. Thibault *et al.*, Phys. Rev. C **12**, 644 (1975); F. Sarazin *et al.*, Phys. Rev. Lett. **84**, 5062 (2000).

[25] M. Anguiano, J.L. Egido and L.M. Robledo, Nucl. Phys. A **683**, 227 (2001); T. Lesinski, T. Duguet, K. Bennaceur and J. Meyer, Eur. Phys. J. A **40**, 121 (2009); H. Nakada and M. Yamagami, Phys. Rev. C **83**, 031302(R) (2011).

[26] A. Poves and J. Retamosa, Phys. Lett. B **184**, 311 (1987); Y. Utsuno, T. Otsuka, T. Mizusaki and M. Honma, Phys. Rev. C **60**, 054315 (1999).

[27] M. Yamagami and N. Van Giai, Phys. Rev. C **69**, 034301 (2004).

[28] J.I. Prisciandaro *et al.*, Phys. Lett. B **510**, 17 (2001).

[29] D. Steppenbeck *et al.*, Nature **502**, 107 (2013).

[30] R. Broda *et al.*, Phys. Rev. Lett. **74**, 868 (1995).

[31] D. Abriola and A.A. Sonzogni, Nucl. Dat. Sheets **109**, 2501 (2008).

[32] T. Sumikama *et al.*, Phys. Rev. Lett. **106**, 202501 (2011).

[33] L.S. Geng, H. Toki and J. Meng, Mod. Phys. Lett. A **19**, 2171 (2004).

[34] N. Nica, Nucl. Dat. Sheets **108**, 1287 (2007).

[35] F.E. Chukreev, V.E. Makarenko and M.J. Martin, Nucl. Dat. Sheets **97**, 129 (2002).

[36] D. De Frenne and E. Jacobs, Nucl. Dat. Sheets **105**, 775 (2005); J. Blachot, Nucl. Dat. Sheets **109**, 1383 (2008).